Supplementary Information for Thirman et. al.

Supplementary Table 1 – Flow cytometry reagents

Reagent	Detect	Clone	Fluorochrome	Manufacturer	Catalog #	Readout	Diversity Set	Roc. Set + Dose Response	Time Course
Antibody	c-CAS3	C96-605	PE	BD Biosciences	550822	Apoptosis [1]	X		X
Antibody	Ki67	B56	BV786	BD Biosciences	563756	Cell proliferation [2,3]		X	
Antibody	p-S6 S235/236	D57.2.2E	Ax594 (Diversity)/Ax647 (37 Roc.)	Cell Signaling Technology	4851S (Diversity)/9865S(37 Roc.)	mTOR+MAPK /ERK activation [4 5]	X	X	
Antibody	p-S6 S240/244	D68F8	Ax488	Cell Signaling Technology	5018S	mTOR activation [4 5]		X	
Antibody	p-AKT S473	D9E	APC	Cell Signaling Technology	11962S	Upstream of mTOR [6,7]			
Antibody	p-LCK Y505	SRRCHA	PerCP-eFluor 710	ThermoFisher Scientific	46-9076-42	Src-family kinase [8]			
Antibody	γH2AX S139	N1-431	PerCP-Cy5.5	BD Biosciences	564718	DNA damage [9]	X	X	X
Antibody	p-STAT3 S727	49/p-Stat3	PE	BD Biosciences	558557	Transcriptional Activity [10]		X	
Antibody	p-STAT5 Y694	SRBCZX	PE-eFluor610	Invitrogen	61-9010-42	Cell survival [11 12]		X	
Antibody	p-ERK T202/Y204	6B8B69	PE-Cy5	Biolegend	369514	MAPK activation [13,14]		X	
Antibody	p-HH3 S28	HTA28	PE-Cy7	Biolegend	641011	M-phase cell cycle [15]	X	X	
Antibody	p-4EBP1 T37/46	236B4	Ax647	Cell Signaling Technology	5123S	Translation [16]		X	
Antibody	p-MLKL	D6H3V	Ax568	Cell Signaling Technology	91689	Necroptosis [17]			X
Antibody	LC3	D3U4C	Ax488	Cell Signaling Technology	13082	Autophagy [18]			X
Antibody	p-EIF2α	119A11	Ax647	Cell Signaling Technology	3597	Unfolded protein response[19]			X
NHS dye	Primary amines		Pacific Blue	ThermoFisher Scientific	P10163		X	X	X
NHS dye	Primary amines		Pacific Orange	ThermoFisher Scientific	P30253		X	X	X
NHS dye	Primary amines		Ax750	ThermoFisher Scientific	A20011		X	X	X
NHS dye	Primary amines		Ax700	ThermoFisher Scientific	A20010		X	X	X

Table lists functional protein states used for measuring specific pathways by flow cytometry, their clone, fluorochrome, vendor source, their role in various intracellular signaling pathways, and the corresponding panel where they were used. Modeled after Balsamo et. al. [19].

Supplementary Table 2 – Positive and negative control compounds

Compound	Source	Catalog #	Conc.	Purpose
Dimethyl sulfoxide (DMSO)	Fisher	BP231-1		Negative control
staurosporine	LKT Labs	S7600	1 μM	c-CAS3 + γH2AX pos. control
etoposide	Cayman Chemicals	33419-42-0	10 μM	γH2AX + c-CAS3 pos. control
CMLD010335	BU-CMD		10 μM	Rocaglate control
rapamycin	LC Labs	NC9163747	0.01 μM	p-S6 suppression pos. control
Nocodazole	Acros	358240100	4 μM	G2 cell cycle arrest + p-HH3 pos. control
aphidicolin	Fisher	AC611970010	4 μM	G1 cell cycle arrest + p-HH3 pos. control

Table lists compounds used as positive and negative controls for specific pathway measurements made by flow cytometry, vendor source, final concentration, and a short description of their purpose.

Thirman et. al. – Supplementary Figure 1

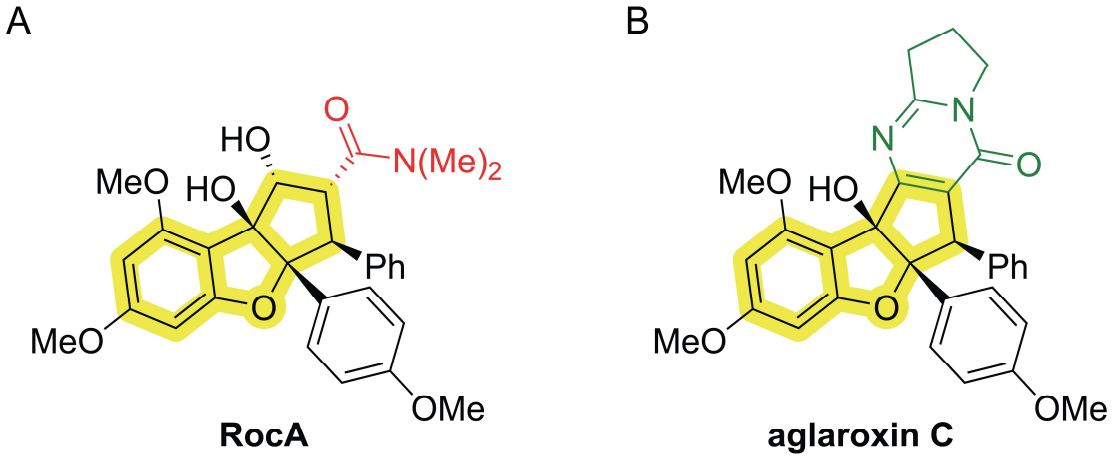

Supplementary Figure 1 – RocA and aglaroxin C are exemplar rocaglates for their respective subclasses. A) Chemical structure for rocaglamide (RocA), a regular rocaglate (RR). R group is colored in red based on classification as RR. **B)** Chemical structure for aglaroxin C, a rocaglate pyrimidinone. Ring fusion is colored in green based on classification as RP.

Thirman et. al. – Supplementary Figure 2

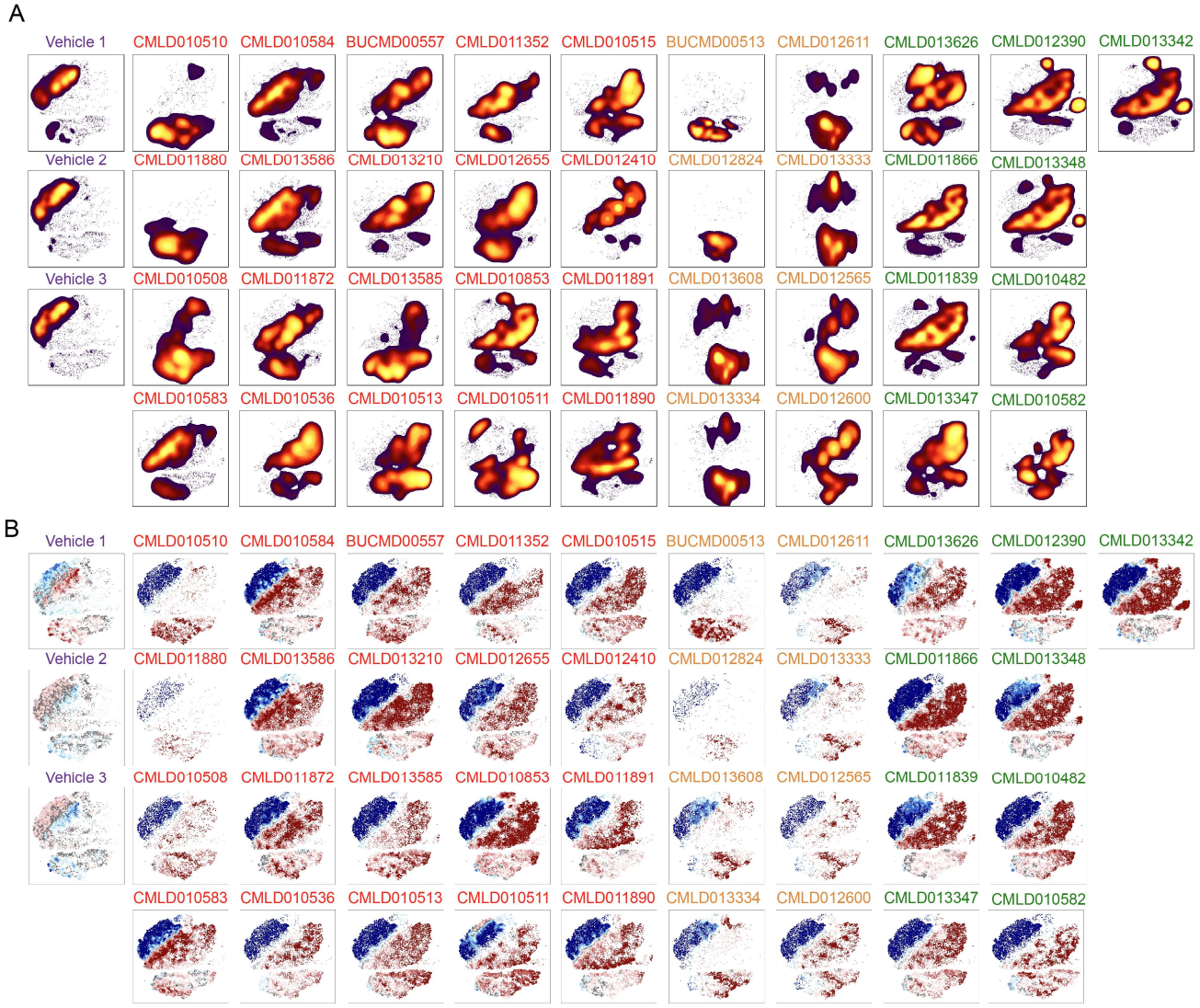

Supplementary Figure 2 - Rocaglates had distinct patterns of bioactivity in leukemia. A) t-SNE plots depicting the result of performing a t-SNE analysis on the entire pre-processed MV411 dataset and dividing based on compound. **B)** T-REX plots depict regions of significant difference between the t-SNE of one compound vs. the pooled set of vehicle-treated cells in MV411. For both **A)** and **B)** compound names are colored according to rocaglate structural subclass.

Thirman et. al. – Supplementary Figure 3

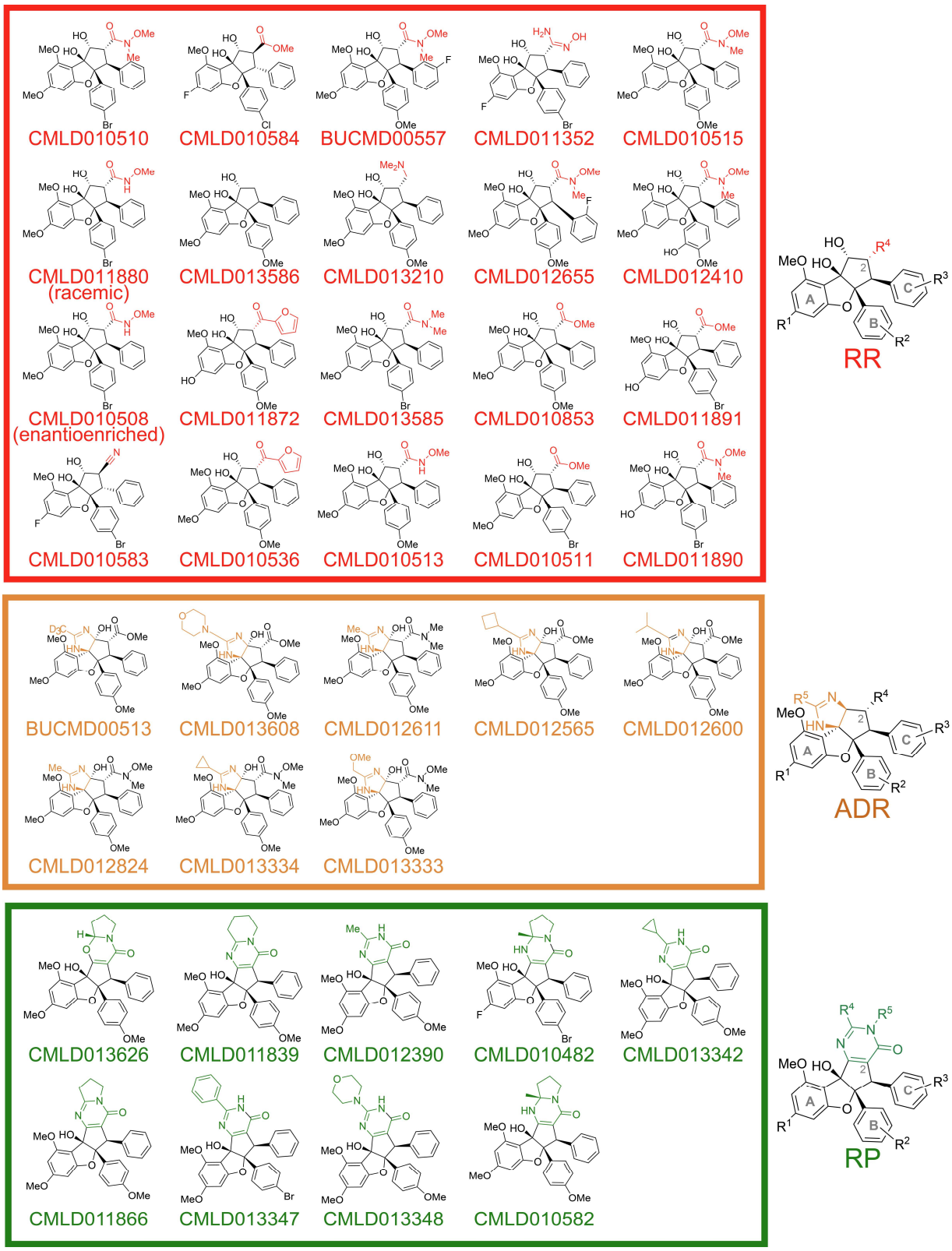

Supplementary Figure 3 - The 37 rocaglates were organized into three structural subclasses. The structures of the 37 rocaglates are organized into boxes according to membership to one of three subclasses. Boxes, compound names, and R groups are colored according to rocaglate subclass. The defining structural scheme for each subclass is shown to the right of each box.

Thirman et. al. – Supplementary Figure 4

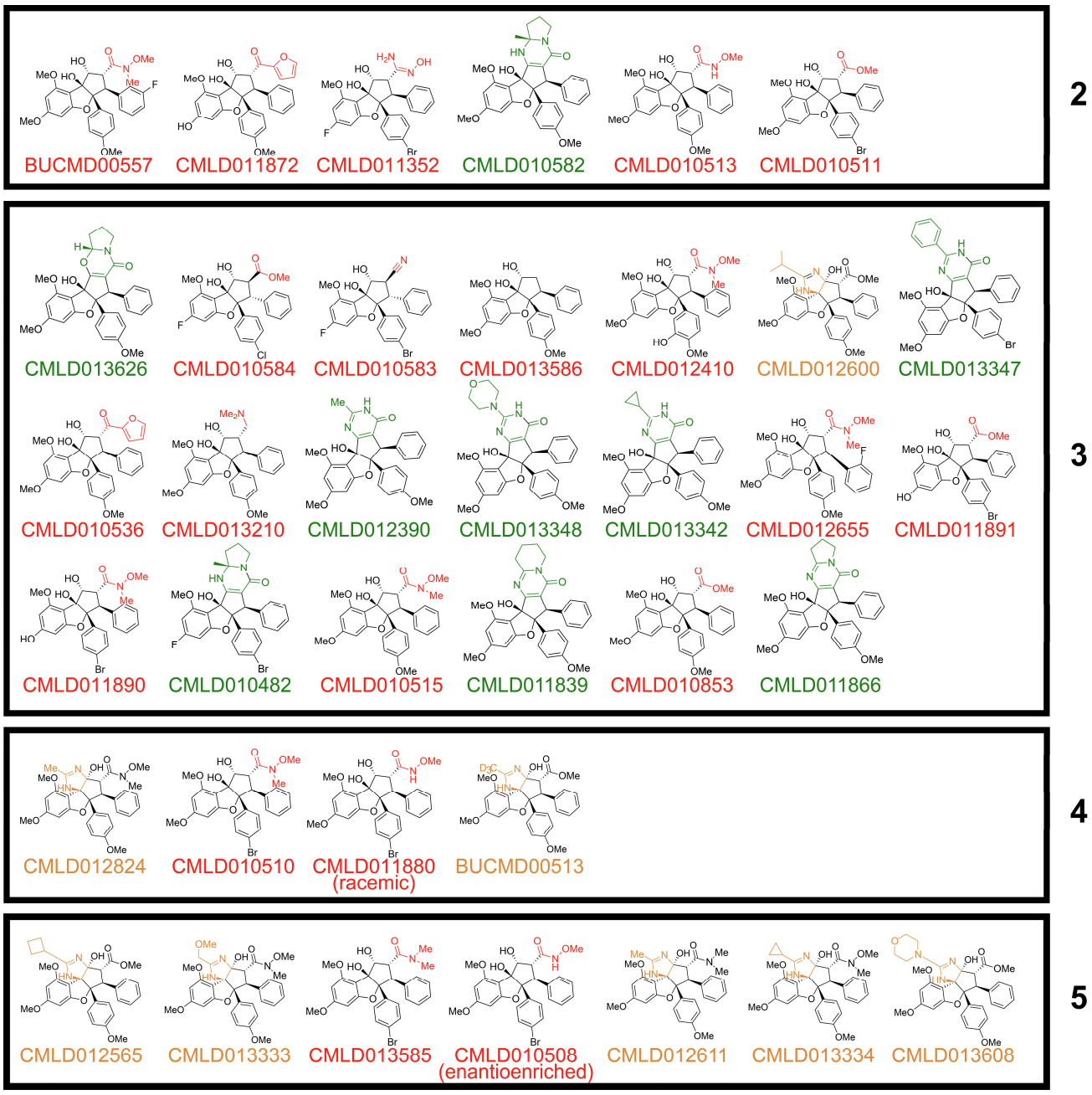

Supplementary Figure 4 – Dendrogram clusters provided deeper insight into potential machine-learned structure-activity relationships. The structures of the 37 rocaglates are organized according to the dendrogram clusters formed based on transformed median fluorescence intensity in **Figure 3B**. Compound names and R groups are colored according to rocaglate structural subclass. The cluster number from **Figure 3B** is listed on the right side of each box.

Thirman et. al. – Supplementary Figure 5

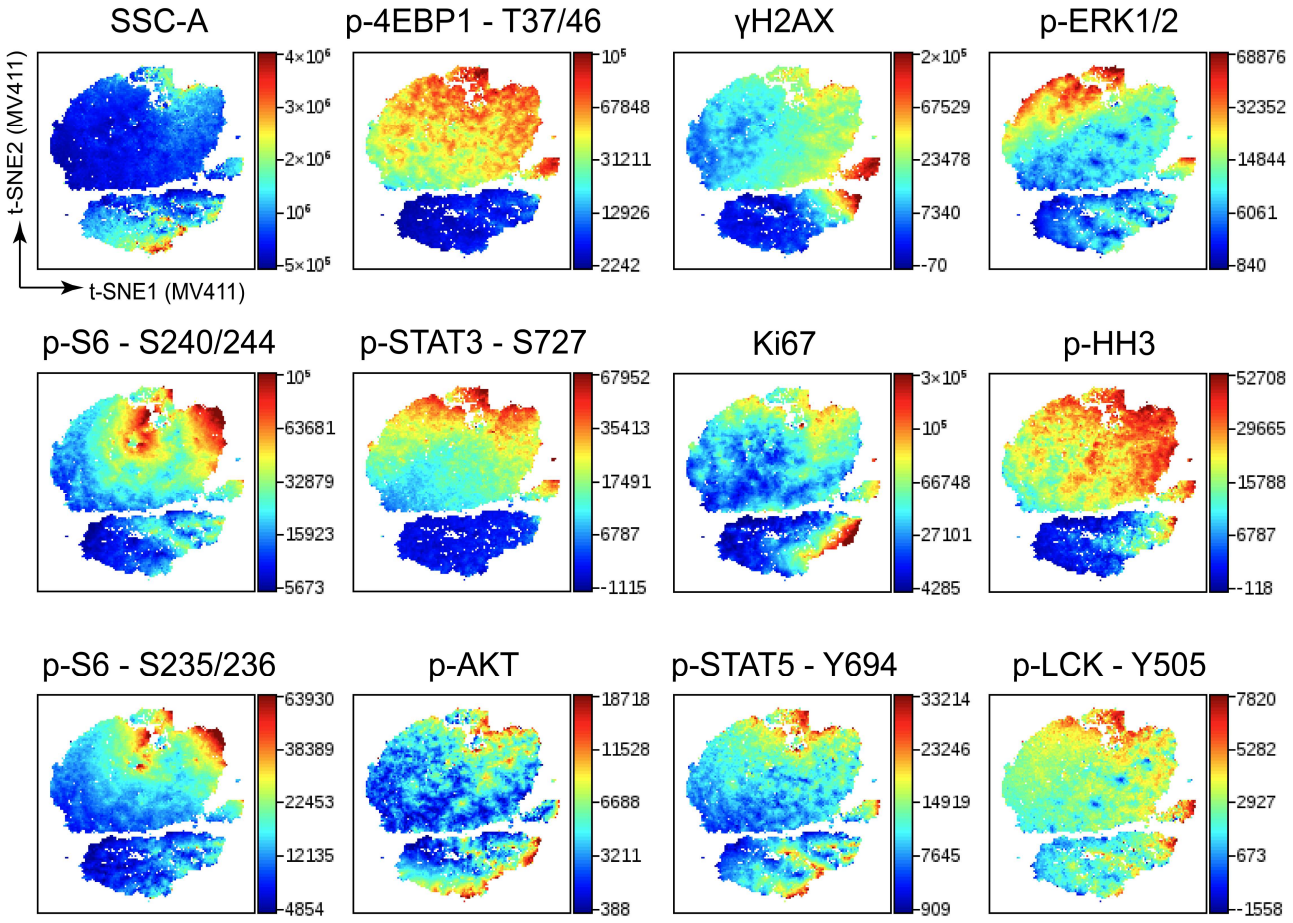

Supplementary Figure 5 - Heterogeneity existed at the single-cell level across functional readouts. Plot depicting the result of performing a t-SNE analysis on the entire pre-processed MV411 dataset and coloring based on protein measurements for each of the 11 functional readouts tested (and SSC-A). Each readout is on its own scale as seen in the legend on the right side of each plot.

Thirman et. al. – Supplementary Figure 6

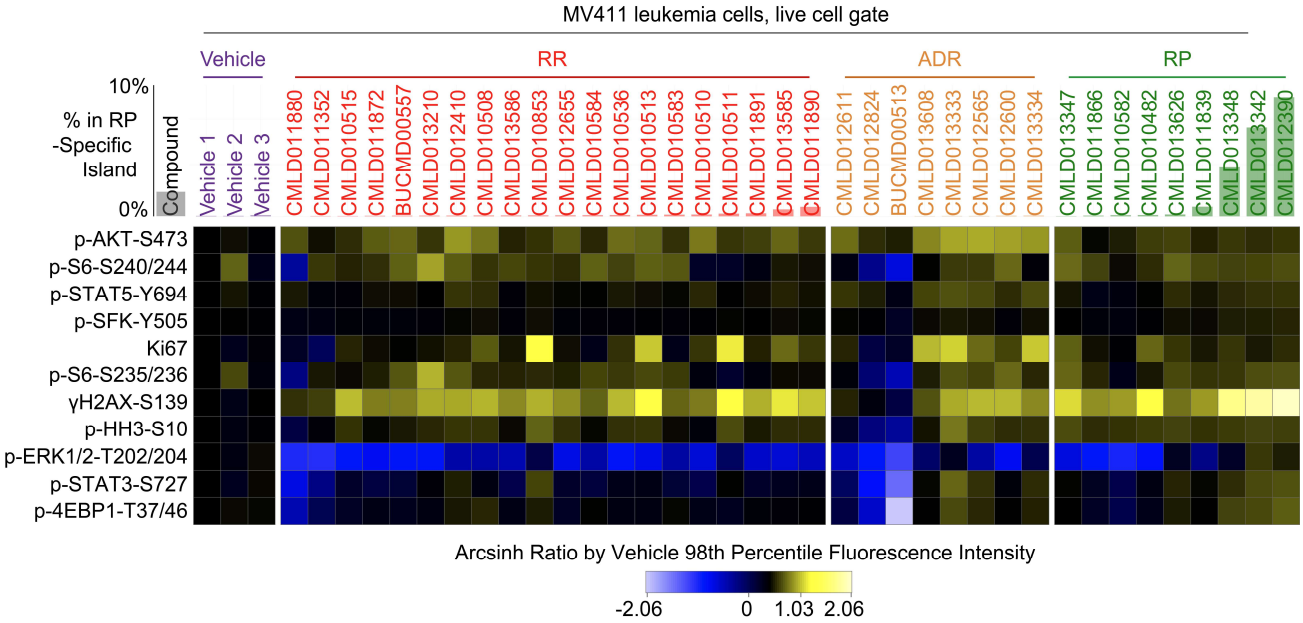

Supplementary Figure 6 – The RP island was associated with high γH2AX and p-4EBP1 and low p-ERK. Heatmap depicting the arcsinh ratio of the 98th percentile fluorescence intensity for each compound (listed on top of heatmap) and readout (listed left of heatmap) by the median fluorescence intensity of Vehicle 1. Cells on the heatmap range from light blue for the lowest values to bright yellow for the highest values. Compounds are grouped and colored according to the rocaglate subclass listed on the top of the plot. A bar plot depicting the percentage of cells in the RP island for each compound is shown behind each respective compound name.

Thirman et. al. – Supplementary Figure 7

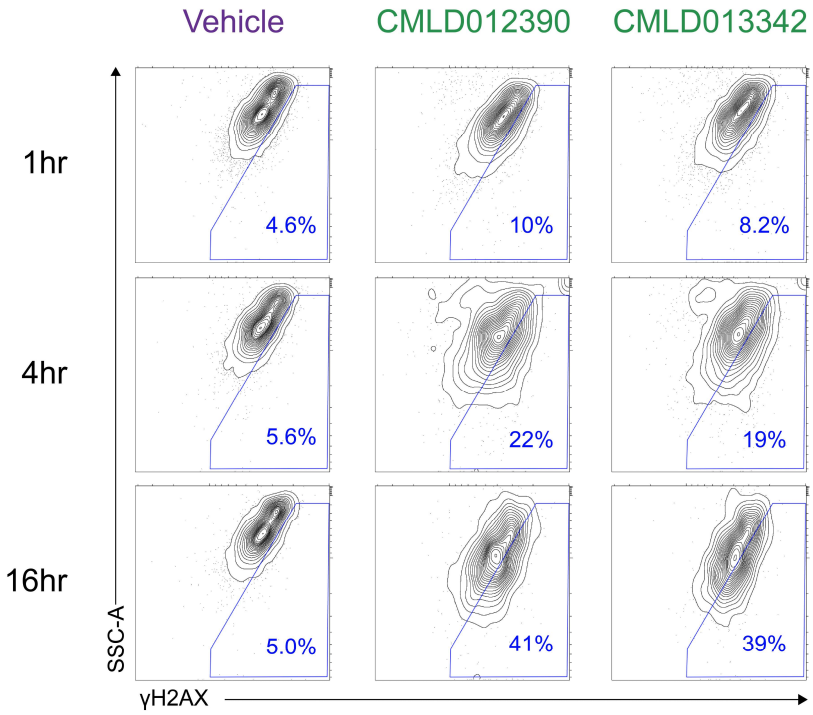

Supplementary Figure 7 - RPs showed γH2AX activation within 4 hours that continued to increase at 16 hours. Contour plots depicting SSC-A vs. γH2AX with 10% of cells per contour. Rows are arranged in order of increasing compound stimulation time. Percentages in the lower right corners of individual plots indicate the percentage of cells within the γH2AX+ polygon gate shown in blue. Compound names at the top of plots are colored based on membership to RP subclass.

References

1 Crowley, L. C. & Waterhouse, N. J. Detecting Cleaved Caspase-3 in Apoptotic Cells by Flow Cytometry. *Cold Spring Harb Protoc* **2016** (2016). https://doi.org:10.1101/pdb.prot087312

2 Uxa, S. *et al.* Ki-67 gene expression. *Cell Death & Differentiation* **28**, 3357-3370 (2021). https://doi.org:10.1038/s41418-021-00823-x

3 Miller, I. *et al.* Ki67 is a Graded Rather than a Binary Marker of Proliferation versus Quiescence. *Cell Rep* **24**, 1105-1112.e1105 (2018). https://doi.org:10.1016/j.celrep.2018.06.110

4 Magnuson, B., Ekim, B. & Fingar, D. C. Regulation and function of ribosomal protein S6 kinase (S6K) within mTOR signalling networks. *Biochem J* **441**, 1-21 (2012). https://doi.org:10.1042/bj20110892

5 Roux, P. P. *et al.* RAS/ERK Signaling Promotes Site-specific Ribosomal Protein S6 Phosphorylation via RSK and Stimulates Cap-dependent Translation *. *Journal of Biological Chemistry* **282**, 14056-14064 (2007). https://doi.org:10.1074/jbc.M700906200

6 Blix, E. S. *et al.* Phospho-specific flow cytometry identifies aberrant signaling in indolent B-cell lymphoma. *BMC Cancer* **12**, 478 (2012). https://doi.org:10.1186/1471-2407-12-478

7 Irish, J. M. *et al.* B-cell signaling networks reveal a negative prognostic human lymphoma cell subset that emerges during tumor progression. *Proc Natl Acad Sci U S A* **107**, 12747-12754 (2010). https://doi.org:10.1073/pnas.1002057107

8 Takata, M. *et al.* Tyrosine kinases Lyn and Syk regulate B cell receptor-coupled Ca2+ mobilization through distinct pathways. *The EMBO Journal* **13**, 1341-1349-1349 (1994). https://doi.org:https://doi.org/10.1002/j.1460-2075.1994.tb06387.x

9 Mah, L. J., El-Osta, A. & Karagiannis, T. C. γH2AX: a sensitive molecular marker of DNA damage and repair. *Leukemia* **24**, 679-686 (2010). https://doi.org:10.1038/leu.2010.6

10 Igelmann, S., Neubauer, H. A. & Ferbeyre, G. STAT3 and STAT5 Activation in Solid Cancers. *Cancers (Basel)* **11** (2019). https://doi.org:10.3390/cancers11101428

11 Wingelhofer, B. *et al.* Pharmacologic inhibition of STAT5 in acute myeloid leukemia. *Leukemia* **32**, 1135-1146 (2018). https://doi.org:10.1038/s41375-017-0005-9

12 Kotecha, N. *et al.* Single-cell profiling identifies aberrant STAT5 activation in myeloid malignancies with specific clinical and biologic correlates. *Cancer Cell* **14**, 335-343 (2008). https://doi.org:10.1016/j.ccr.2008.08.014

13 Roskoski, R., Jr. ERK1/2 MAP kinases: structure, function, and regulation. *Pharmacol Res* **66**, 105-143 (2012). https://doi.org:10.1016/j.phrs.2012.04.005

14 Mendoza, M. C., Er, E. E. & Blenis, J. The Ras-ERK and PI3K-mTOR pathways: cross-talk and compensation. *Trends Biochem Sci* **36**, 320-328 (2011). https://doi.org:10.1016/j.tibs.2011.03.006

15 Hans, F. & Dimitrov, S. Histone H3 phosphorylation and cell division. *Oncogene* **20**, 3021-3027 (2001). https://doi.org:10.1038/sj.onc.1204326

16 Gingras, A. C. *et al.* Regulation of 4E-BP1 phosphorylation: a novel two-step mechanism. *Genes Dev* **13**, 1422-1437 (1999). https://doi.org:10.1101/gad.13.11.1422

17 Pasparakis, M. & Vandenabeele, P. Necroptosis and its role in inflammation. *Nature* **517**, 311-320 (2015). https://doi.org:10.1038/nature14191

18 Runwal, G. *et al.* LC3-positive structures are prominent in autophagy-deficient cells. *Sci Rep* **9**, 10147 (2019). https://doi.org:10.1038/s41598-019-46657-z

19 Balsamo, J. A. *et al.* An immunogenic cell injury module for the single-cell multiplexed activity metabolomics platform to identify promising anti-cancer natural products. *J Biol Chem* **298**, 102300 (2022). https://doi.org:10.1016/j.jbc.2022.102300